RSC Advances

ROYAL SOCIETY OF CHEMISTRY

www.rsc.org/advances

Cite this: DOI: 10.1039/c0xx00000x

www.rsc.org/xxxxxx

ARTICLE TYPE

Fabrication of highly durable hydrophobic PBZ/SiO_2 surfaces

A.Shakila Parveen, P. Thirukumaran and M. Sarojadevi*

Received (in XXX, XXX) Xth XXXXXXXXX 20XX, Accepted Xth XXXXXXXXX 20XX
DOI: 10.1039/b000000x

Abstract

The structure of the synthesized precursors [4-phenyl (diazenyl) phenol (PAP)] & [N,N'-bis(4-aminophenyl) terephthalamide (APTA)] and benzoxazine monomer [bis (6-phenyl diazenyl-3,4-dihydro-2H-1,3-benzoxazinyl) terephthalamide (BZO-TA)] were confirmed by Fourier Transform Infrared (FT-IR) and Nuclear Magnetic Resonance (^{1}H & ^{13}C-NMR) spectroscopy. The miscibility and curing behaviour of the SiO_2 nanoparticles with benzoxazine was examined by Differential Scanning Calorimetric (DSC) analysis. Polybenzoxazine – silica nano hybrids [PBZ:SiO_2] with different weight ratios of SiO_2 nanoparticles (1, 3 and 5 wt%) were prepared by thermal curing method. Surface morphological studies from SEM (Scanning Electron Microscopy) and AFM (Atomic Force Microscopy) revealed that the PBZ:SiO_2 hybrids at same compositions show hierarchical structured roughness. FT-IR was used to investigate the thermal-curing reactions and hydrogen bonding interactions in both polybenzoxazine and its hybrids. Contact angle analysis indicated that the hybrids have hydrophobic nature and low wettability. Thermal and mechanical stability of the hybrids were studied using Thermogravimetric (TGA) and Dynamic Mechanical Analysis (DMA).

Keywords: Polybenzoxazine, SiO_2 nanoparticles, hydrogen bonding interactions, hydrophobicity.

.

Introduction

Water repellency is an important property of a material and is one of the most challenging subjects for both fundamental research and practical applications[1,2]. The hydrophobicity of a surface can be improved by controlling its surface chemical composition (surface area) and topographical microstructure (surface roughness). Hierarchial surface roughness possessing both nanometer and micrometer sized particles is an effective approach to create hydrophobic/superhydrophobic surfaces. Surface roughness plays an important role in preparing these surfaces as explained by Wenzel and Cassie. According to them, an increase in surface roughness increases the surface area of the material and thus enhances its hydrophobicity. Moreover, due to the surface roughness, air becomes trapped within the grooves beneath the liquid and since air is an absolutely hydrophobic material (CA = 180 ^{o}), the liquid drop sits partially on air leading to a superhydrophobic surface[3-5]. Several fabrication methods like inorganic particle deposition, sol-gel techniques, plasma treatments, chemical etching, electrospinning and casting techniques were used to prepare superhydrophobic surfaces. Generally, surface with high roughness has poorer mechanical strength when compared with a flat surface. A lack of mechanical durability is a common problem for most of the hydrophobic surfaces that limits its potential applications[1,5-7].

The performance of polymeric materials is often dictated by their surface properties, such as wettability, friction and adhesion. A low surface energy is important for many practical applications of polymers8. Polybenzoxazine (PBZ) is a novel class of phenolic resin that has been developed recently to overcome several shortcomings of the traditional phenolic resins9-11. It is a class of low surface free energy (SFE) materials with a wide range of interesting features including near-zero volumetric change upon curing, low degree of water absorption, high char yeild, high glass-transition temperature, excellent resistance to chemicals, excellent electrical properties and high thermal stability. This kind of thermoset resin possesses low surface free energy [16.4 mJ/m_2] than that of Teflon [21.0 mJ/m $_2$][3,5-6]. The films prepared by these benzoxazine monomers possess several merits: i) the films synthesized by using conventional raw materials cost less ii) the polybenzoxazine films with low surface free energy were produced by single-step thermal curing process. In recent years, much efforts have been exerted in the search for low-cost polymeric materials exhibiting low surface free energies, ready processability and good film-forming characteristics.[8,12].

Over the past few years, 2,2-bis(3,4-dihydro-3-methyl-2H-1,3-benzoxazinyl) propane [BA-m], 2,2-bis(3-phenyl, 3,4-dihydro-2H-1,3-benzoxazinyl) propane [BA-a] and 2,2-bis(3-fluorophenyl, 3,4-dihydro-2H-1,3-benzoxazinyl) hexafluoro propane [BAF-fa] were reported as low surface energy materials. Wang et al. reported that polybenzoxazines (PBZs) are a new class of low surface free energy polymeric materials. They also found that the surface energies of the polybenzoxazines generally decrease upon increasing the curing time due to the formation of strong intramolecular hydrogen bonding of six membered rings [6,8]. It is believed that incorporation of SiO_2 nanoparticles into the polybenzoxazine network structure will result in excellent heat resistance, flame resistance and mechanical performance. This kind of polybenzoxazine – SiO_2 hybrid is prepared by a simple thermal curing method, and has the potential to be applied as low-cost hydrophobic material [11,3]

In this contribution, we report a simple but effective approach to fabricate highly hydrophobic surfaces based on polybenzoxazine incorporated with SiO_2 nanoparticles by thermal curing method. The PBZ – SiO_2 hybrids with rough surfaces possessing both hierarchial macro and nano scaled structures are reported in this paper.

Experimental

Materials

Paraformaldehyde, aniline, dimethylsulfoxide (DMSO), tetrahydrofuran (THF), N,N- dimethylformamide (DMF) and ethanol were purchased from E-Merck Limited, India; potassium carbonate (K_2CO_3), sodium nitrite ($NaNO_2$) and phenol were purchased from s d fine – chem limited, Inida; silica nanoparticles (particle size 20-30 nm), 4-nitroaniline and terephthaloyl chloride were purchased from Alfa Aesar (Johnson Mathew Company), India, Pvt. Ltd.; hydrazine monohydrate and dichlorodimethyl silane were purchased from Spectrochem Pvt. Ltd., India; 10% Pd/C was purchased from Sisco Research Laboratories, Pvt. Ltd., India. All chemicals and solvents were used without further purification.

Characterization

Fourier transform infrared (FT-IR) spectra of the samples were obtained using an ABB Bomem (Model MB 3000) spectrometer. The samples were ground with spectroscopy grade KBr and made into pellets. ^{1}H (500 MHz) & ^{13}C (125 MHz) nuclear magnetic resonance (NMR) spectra were recorded on a Jeol Spectrometer with tetramethylsilane (TMS) as the internal standard, in $CDCl_3$. Differential scanning calorimetry (DSC) was performed in a TA instrument Q10 model using 5-10 mg of the sample at a heating rate of 10^{o}C/min in nitrogen atmosphere. The morphology of the material was examined by scanning electron microscope (SEM) (JEOL, JSM-5600) at an accelerating voltage of 20 kV. The surface topology (roughness) of the fractured surface was investigated by means of atomic force microscopy (AFM) Seiko SPI3800N, series SPA-400 (Tokyo, Japan). Contact Angle Measurements were carried out using Goniometer: Digidrop GBX (contact angle meter). Dynamic mechanical analysis (DMA) was carried out using a Netzsch 242 DMA at a heating rate of 10^{o}C/min from 30 to 250^{o}C. Thermo gravimetric analysis (TGA) was performed using a TA Q 600 thermal analyzer. Cured samples were analyzed in open silicon pan at a heating rate of 20^{o}C/min in N_2 atmosphere, up to a maximum temperature of 800^{o}C.

Synthesis of 4-(phenyl diazenyl) phenol [PAP]

In a three necked round bottomed flask fitted with a magnetic stirrer, conc. HCl (8 mL) and deionised water (8 mL) were taken. This solution was cooled to 0 ^{o}C and aniline (2.5 g, 2.7 mmol) was added. Then, $NaNO_2$ (2 g, 2.9 mmol) in 10 mL of water was added to the cooled solution with heat control, keeping the solution temperature below 10 ^{o}C. After complete addition, the solution was allowed to stirr for 20 min in ice-bath. Then, separately phenol (2.5 g, 2.7 mmol) was dissolved in 25 mL of 10% NaOH solution. This prepared solution was added slowly to the diazonium salt containing solution under stirring, keeping the temperature below 15 ^{o}C, and stirred for another 45 min. The formed yellow-orange solid [PAP] was filtered and washed with water[14]. The raw solid was crystallized from ethanol/water mixture [Scheme 1]. Yield: 80%.

Scheme 1: Synthesis of 4-phenyl diazenyl phenol [PAP]

FT-IR (KBr, cm^{-1}): 3468 (–OH stretching), 1458 (stretching vibrations of trans N=N), 1373 (C-O stretching), 1281 (C-N stretching), 3070 (C-H stretching vibrations), 1589 (C=C stretching vibrations) and 848 (C-C bending vibrations); ^{1}H-NMR ($CDCl_3$, ppm): 3.8 (s, H_a ,1H). 6.5–8.0 (m, aromatic protons); ^{13}C-NMR ($CDCl_3$, ppm): 164 (C_1), 145 (C_4), 147(C_5), 115-160 (aromatic carbons).

Synthesis of N,N'-bis(4-aminophenyl) terephthalamide [APTA]

4-nitroaniline (13.8 g, 0.1 mol) and terephthaloyl chloride (10.2 g, 0.05 mol) were taken in a 500 mL three necked round bottomed flask fitted with a reflux condenser and magnetic stirrer. 100 mL of DMF and potassium carbonate (13.8 g, 0.1 mol) were added to this mixture and heated to 140 ^{o}C under N_2 atmosphere while stirring. The mixture was maintained at this temperature for 8 h, cooled and then poured into 300 mL of deionised water. The yellow solid [N,N'-bis(4-nitrophenoxy) terephthalamide] [NPTA] obtained was separated by filteration and dried at 70 ^{o}C. Yield: 84%

Nitro compound [NPTA] (4.1 g, 0.01 mol), Pd/C (0.12 g, 3 wt% of NPTA) and ethanol (60 mL) were taken in a 500 mL three necked round bottomed flask fitted with a reflux condenser and magnetic stirrer. To this mixture hydrazine hydrate (15 mL of 85%) was added dropwise over a period of 1 h at reflux temperature. The reaction was continued for about 5 h under reflux conditions. The solution was then filtered to remove the catalysts, cooled to room temperature and then filtered to obtain white crystals[15] of APTA [Scheme 2]. Yield: 82%,

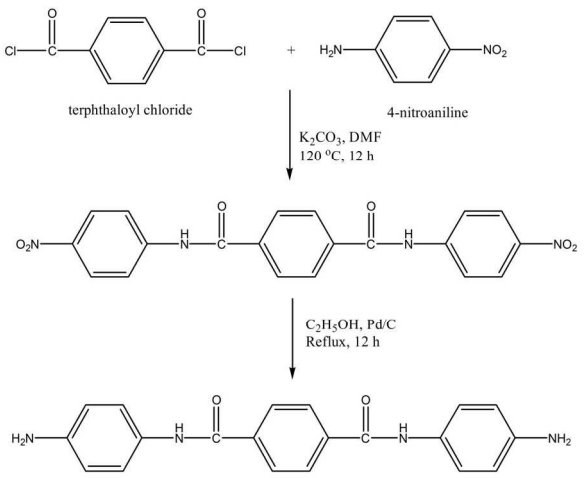

Scheme 2: Synthesis of N,N'-bis(4-aminophenyl) terephthalamide [APTA]

FT-IR (KBr, cm^{-1}): 3348 & 3279 (asymmetric and symmetric stretching vibrations of NH_2), 1643 (C-O stretching), 3433 (N-H stretching), 1427 (C-N stretching), 1450 and 3070 (C=C and C-H stretching vibrations), 779 (bending vibrations of C-H); ^{1}H-NMR ($CDCl_3$, ppm): 3.5 (s, H_a ,4H). 7.3 (s, H_b, 2H), 6.5–8.0 (m, aromatic protons); ^{13}C-NMR ($CDCl_3$, ppm): 167 (C_3), 140 (C_7), 115–160 (aromatic carbons).

Synthesis of bis(6-phenyl diazenyl-3,4-dihydro-2H-1,3-benzoxazinyl) terephthalamide [BZO-TA]

In a 250 mL round bottomed three necked flask equipped with a reflux condenser and magnetic stirrer, para formaldehyde (1.8 g, 0.06 mol) and 50 mL of DMSO were taken and the temperature was increased to 100 °C. Then, synthesized diamine [APTA] (3.5 g, 0.01 mol) and phenol [PAP] (3.9 g, 0.02 mol) were added to the solution and the mixture was heated to 130 °C for 5 h in an oil bath. After which, the solution was cooled to room temperature and poured into 1 L of 1N NaOH solution. The precipitate thus formed was collected by filteration, washed several times with water and finally dried at 60 °C in vacuum to afford BZO-TA as a brown powder[6,15] [Scheme 3]. Yield: 85% m.p. 85.0 (from DSC).

FT-IR (KBr, cm^{-1}): 936 (stretching of oxazine ring), 1231 & 1019 (asymmetric and stretching of C-O-C), 1151 (stretching of C-N-C), 1326 (CH_2 wagging), 3433 (N-H stretching), 2222 (C-N stretching), 1643(C=O stretching), 1456 (trans N=N stretching vibration); ^{1}H-NMR ($CDCl_3$, ppm): 5.4 (s, H_a, 4H), 4.6 (s, H_b, 4H), 7.3 (s, H_c, 2H), 6.5–8.0 (m, aromatic protons); ^{13}C-NMR ($CDCl_3$, ppm): 79 (C_8), 48 (C_9), 167 (C_3), 115–160 (aromatic carbons).

Preparation of PBZ/SiO_2 nanohybrids

For the preparation of PBZ:S1 nanohybrid (1 wt% of SiO_2), 0.5 g of the benzoxazine monomer [BZO-TA] and 0.005 g of SiO_2 nanoparticles were taken in a 100 mL beaker and to this mixture THF (5 mL) was added and it was stirred for 30 min. Then, the solution was poured into a petridish (treated with dichloro

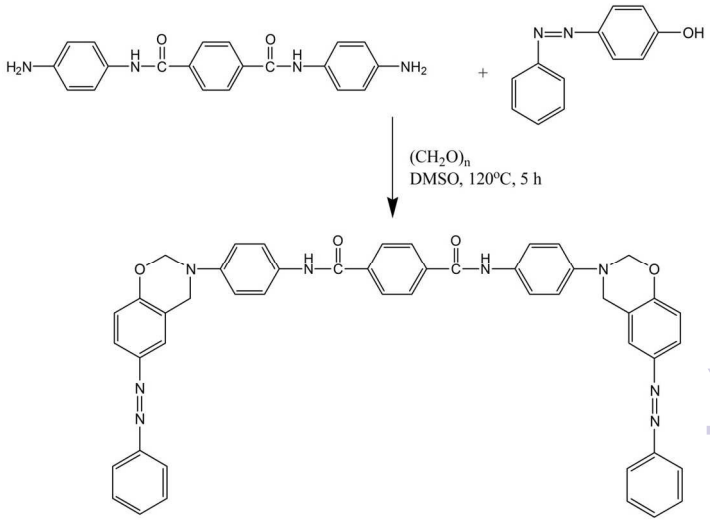

Scheme 3: Synthesis of bis(6-phenyl diazenyl-3,4-dihydro-2H-1,3-benzoxazinyl) terephthalamide [BZO-TA]

dimethyl silane) and heated to 250 °C for 3 h to obtain PBZ:S1 nanohybrid. In a similar way all the other hybrids [PBZ:S0, PBZ:S3 and PBZ:S5] were prepared by varying the silica content.

Results and Discussions

Structural analysis of PAP, APTA and BZO-TA

Synthesized diamine [APTA], phenol [PAP] and para formaldehyde were reacted in the presence of DMSO to form amide and azo functionalized benzoxazine through Mannich condensation reaction. The chemical structure of the synthesized precursors and benzoxazine monomer were confirmed by FT-IR, ^{1}H- and ^{13}C-NMR spectroscopic analysis.

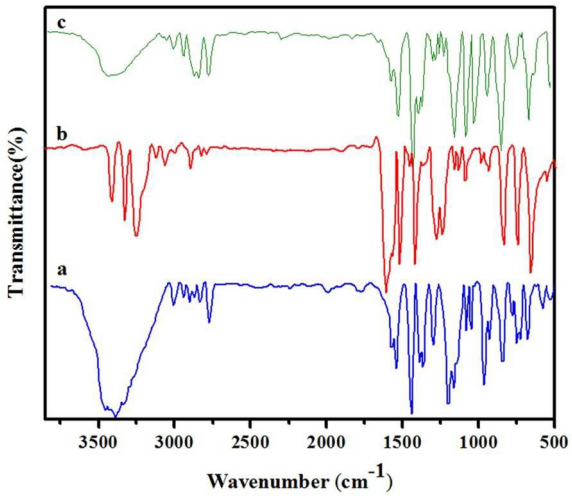

Figure 1: FT-IR spectra of a) PAP b) APTA and c) BZO-TA

Figure 1a shows the FT-IR spectrum of 4-phenyl azenyl phenol. The spectrum shows a broad absorption at 3468 cm^{-1}, due to the

presence of –OH group. The N=N stretching of the azo group is typically located at 1458 cm^{-1} (stretching of trans N=N). Whereas, the absorption bands of C-O and C-N, which are attached with the benzene ring are observed at 1373 and 1281 cm^{-1} respectively[16-18]. Moreover, the characteristic frequencies of the aromatic ring are observed at 3070, 1589 and 848 cm^{-1}, which are attributed to C-H stretching, C=C stretching and C-C bending vibrations, respectively. Figure 1b represents the FT-IR spectrum of the synthesized diamine [APTA]. The absorptions due to asymmetric and symmetric stretching vibrations of the diamine[19] are located at 3348 and 3279 cm^{-1}. The characteristic absorptions of the amide group appear at 1643 cm^{-1} for –C=O group, at 3433 cm^{-1} for –NH group and at 1427 cm^{-1} for C–N group respectively. The C=C stretching, C-H stretching and C-H bending vibrations of the aromatic rings appear at 1450, 3070 and 779 cm^{-1} respectively. The FT-IR spectrum of the synthesized benzoxazine monomer [BZO-TA] is shown in Figure 1c. The characteristic absorption band of the benzoxazine ring appears at 936 cm^{-1} due to the out of plane bending vibrations of C-H of the oxazine ring. Moreover, the other characteristic absorption bands of the benzoxazine ring appear at 1231 cm^{-1} (asymmetric stretching of C-O-C), 1019 cm^{-1} (symmetric stretching of C-O-C), 1151 cm^{-1} (stretching of C-N-C) and 1326 cm^{-1} (CH_2 wagging). Absorption bands around 3433, 2222 and 1643 cm^{-1} are attributed to N-H, C-N and C=O stretches of the amide group respectively. Moreover, the band observed at 1456 cm^{-1} corresponds to trans N=N stretching vibratin of the azo group[20-23].

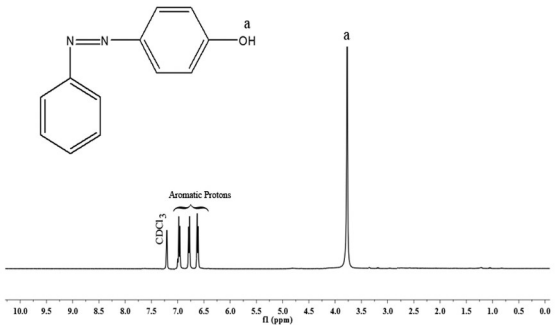

Figure 2: ^{1}H-NMR spectrum of PAP.

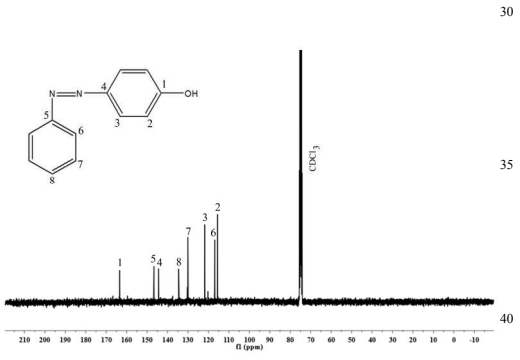

Figure 3: ^{13}C-NMR spectrum of PAP

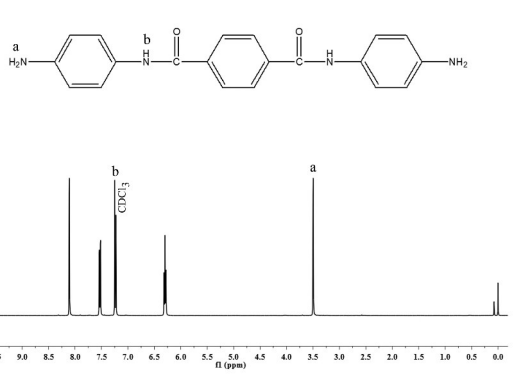

Figure 4: ^{1}H-NMR spectrum of APTA

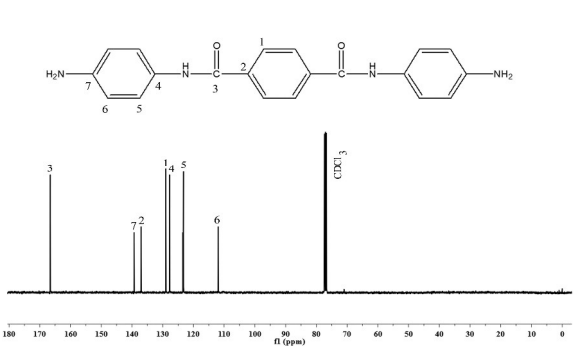

Figure 5: ^{13}C-NMR spectrum of APTA

The ^{1}H- and ^{13}C-NMR spectra of PAP are given in figures 2 and 3. In Fig. 2, there is a singlet at 3.8 ppm due to the –OH proton (H_a). Aromatic protons appear in the range of 6.5 – 7.0 ppm. There is a peak at 7.2 ppm due to the solvent ($CDCl_3$). The ^{13}C-NMR spectrum (Fig. 3) shows a peak at 164 ppm, due to the resonance of the aromatic carbon (C_1) attached to the hydroxyl group. Whereas, the carbons that are attached to the azo group (C_4 & C_5) gave resonance peaks at 145 and 147 ppm. All the other aromatic carbons resonate between 115 – 135 ppm. The ^{1}H- and ^{13}C-NMR spectra of diamine [APTA] are shown in Figures 4 and 5. The presence of amino protons (H_a) and amide protons (H_b) is confirmed by the singlets at 3.5 and 7.3 ppm respectively (Fig. 4). The aromatic protons appear between 6.2 and 8.4 ppm, respectively. In case of ^{13}C-NMR (Fig. 5), the carbonyl carbons (C_3) gave peak at 167 ppm. Moreover, the aromatic carbon attached to amino group (C_7) gave peak at 140 ppm. All the other aromatic carbons resonate between 112 and 138 ppm, respectively[14].

The structure of the benzoxazine monomer [BZO-TA] is confirmed by ^{1}H- and ^{13}C-NMR as shown in Figures 6 and 7 respectively. The existence of oxazine ring protons (H_a, O-CH_2-N) and (H_b, Ar-CH_2-N) is indicated by two singlets (Fig. 6) at 5.4 and 4.6 ppm respectively. The peak at 7.2 ppm represents the N-H protons of the amide group (H_c). Other protons corresponding to the aromatic ring are located between 6.7 and 8.0 ppm respectively. Furthermore, the absence of peaks around 3.1 and 3.6 ppm (due to the open structure of oxazine ring) confirms the structure of benzoxazine

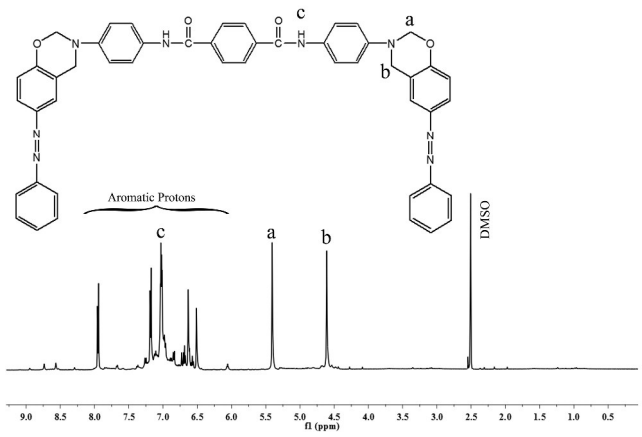

Figure 6: ^{1}H-NMR spectrum of BZO-TA

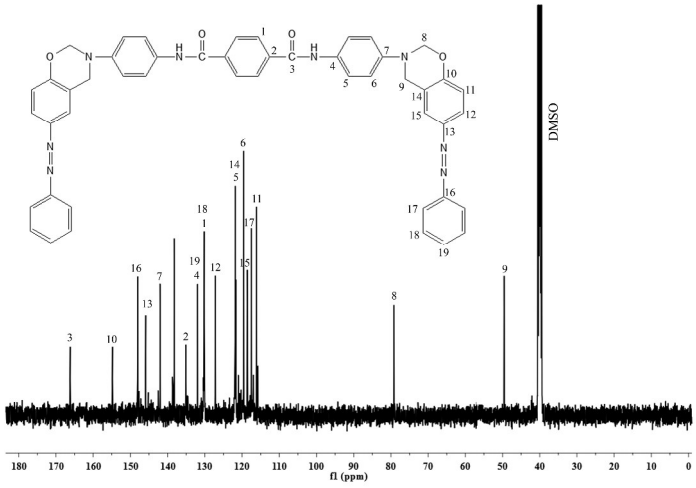

Figure 7: ^{13}C-NMR spectrum of BZO-TA.

monomer. In the 13C-NMR spectrum (Fig. 7), the peaks due to the oxazine ring carbons (C_8, O-CH_2-N) and (C_9, Ar-CH_2-N) appear at 79 and 48 ppm, respectively. The peak at 167 ppm is due to the carbonyl carbon (C_3). And the peaks corresponding to other aromatic carbons appear in the range of 115 – 156 ppm, respectively. All the above mentioned data confirm the structures of PAP, APTA and BZO-TA[20-23].

Curing behavior of BZO-SiO_2 hybrids

The curing behavior of the benzoxazine monomer and benzoxazine – nano SiO_2 hybrids was investigated using DSC & FT-IR. The representative DSC thermograms and FT-IR spectra are presented in Figures 8 and 9 respectively. Figure 8 shows endothermic peaks between 85.0 and 86.5 ^{o}C which are attributed to the melting point of the monomer and its hybrids with SiO_2 nanoparaticles. For the benzoxazine monomer, an exothermic peak appeared with an onset temperature of 130 ^{o}C and a peak temperature of 163 ^{o}C, indicating that ring – opening polymerization has occurred[6]. For the BZO-SiO_2 hybrids a single exotherm is detected with onset and maximum curing temperature in the range of 132 – 149 ^{o}C and 167 – 175 ^{o}C, respectively[8]. This shows the miscibility of the nano SiO_2 with the benzoxazine monomer. Futhermore, the area under the exothermal peaks (ΔH) decreased upon increasing the SiO_2 content from 343 J/g [for neat BZO] to 211 J/g [BZO:S5] [Table 1]. This means that the heat liberated during curing decreases as the ratio of BZO monomer in the hybrids decreases[22].

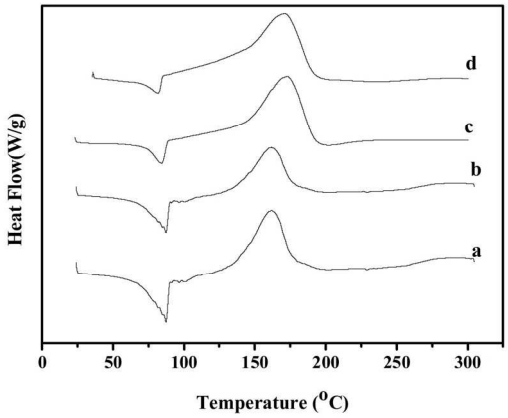

Figure 8: DSC thermograms of BZO-SiO_2 hybrids a) BZO:S0; b) BZO:S1; c) BZO:S3 and d) BZO:S5

The curing reaction of the benzoxazine monomer and its hybrids with nano – SiO_2 was further confirmed by FT-IR analysis. Figure 9 shows the FT-IR spectra of BZO/SiO_2 [9A] & PBZ/SiO_2 [9B] hybrids. Generally, the curing process proceeds via the cleavage of C-O-C bond in the oxazine ring. The characteristic absorption bands of the oxazine ring at 936, 1231, 1019 and 1151 cm^{-1} disappeared (Fig. 9B) after curing at 250 ^{o}C for 3 h. At the same time, there is a broad absorption band around 3400 – 3500 cm^{-1}, which is ascribed to the stretching vibration of hydrogen bonded phenolic hydroxyl groups. Furthermore, the absence of shoulder band at 3626 cm^{-1} clearly indicates that there is no free hydroxyl group either in PBZ or in PBZ/SiO_2 hybrids. A new band appears at 1480 cm^{-1} for the tetrasubstituted aromatic ring of polybenzoxazine. In addition to it in Figure 9B (b-d) there are two absorption bands, one around 1142 – 1126 cm^{-1} and the other around 1041 – 1026 cm^{-1} due to stretching vibrations of Si-O-Si and Si-O-C bond, whose intensity increases upon increasing SiO_2 contents. All the above mentioned changes in the FT-IR spectra are consistent with the formation of polybenzoxazine network via oxazine ring opening polymerization as well as benzoxazine/SiO_2 hybrid systems in the neat benzoxazine matrix[11-13] [Scheme 4].

S.No	Samples	SiO_2 (wt%)	T_{onset} (^{o}C)	T_{max} (^{o}C)	T_{final} (^{o}C)	ΔH (J/g)
1.	BZO:S0	0	130	163	175	343
2.	BZO:S1	1	132	167	181	297
3.	BZO:S3	3	143	172	193	290
4.	BZO:S5	5	149	175	197	210

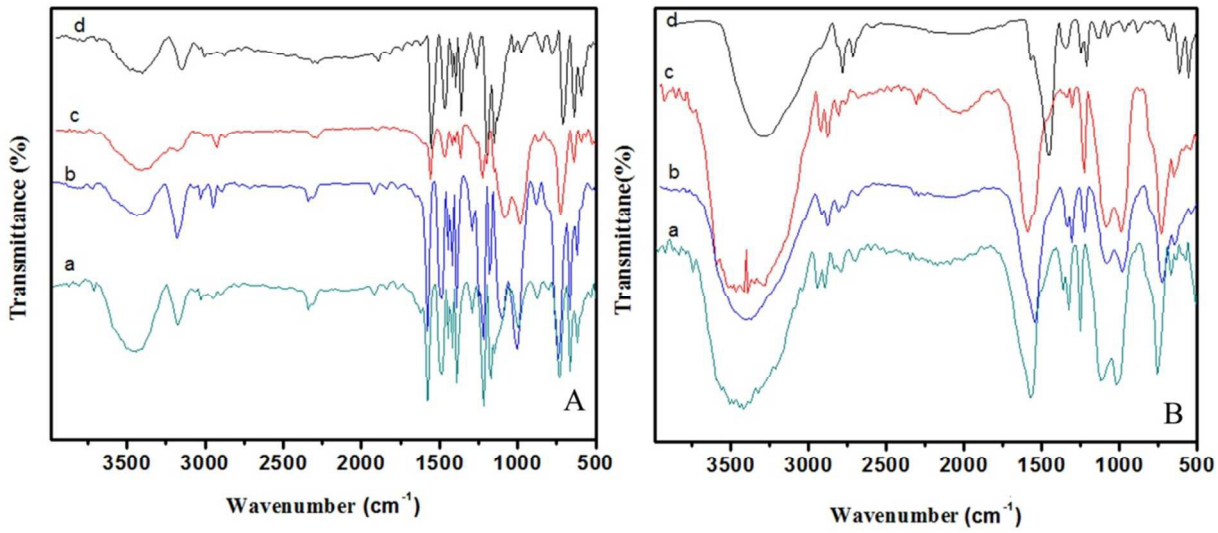

Figure 9: FT-IR spectra of BZO-SiO_2 hybrids [9A] a) BZO:S0; b) BZO:S1; c) BZO:S3 and d) BZO:S5 & PBZ-SiO_2 hybrids [9B] a) PBZ:S0; b) PBZ:S1; c) PBZ:S3 and d) PBZ:S5

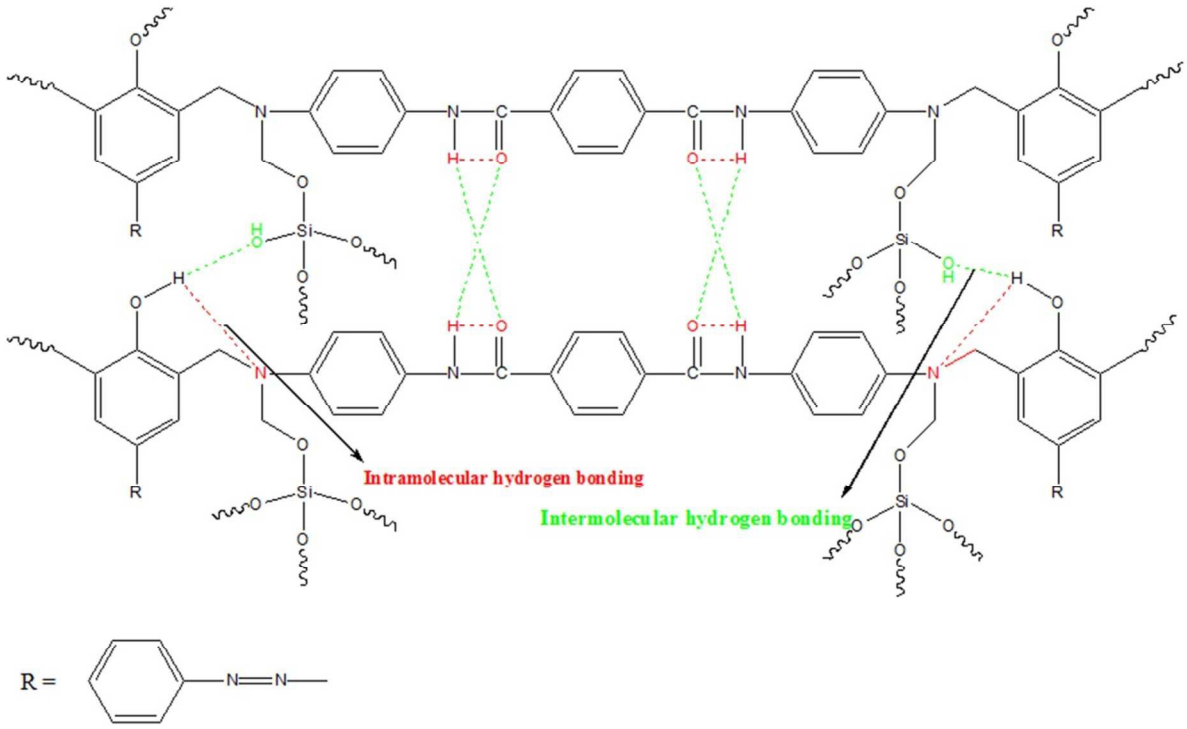

Scheme 4: Structure of PBZ/SiO2 hybrid showing inter- and intramolecular hydrogen bonding

Hydrogen bonding interactions

FT-IR measurement was used to identify the hydrogen bonding interactions between the polybenzoxazine macromolecules and silica nanoparticles. In Figure 9, the region between 2500 – 4000 cm^{-1} was selected to explain the different types of hydrogen bonding for the benzoxazine, polybenzoxazine and PBZ/SiO_2 hybrids. Benzoxazine monomer and its hybrids are thermally cured via oxazine ring – opening polymeriation at 250 ^oC, which results in the formation of network structure with phenolic hydroxyl groups[6]. These hydroxyl groups interact with the hetero atoms within the same network and the silica nanoparticles through intra and intermolecular hydrogen bonding. In the case of benzoxazine monomer [Fig. 9A (a)], there is only intramolecular hydrogen bonding [NH…….O] between the amide [O=C-NH] groups which appear at 3194 cm^{-1}. Whereas for the polymer [Fig. 9A (a)] and its nanohybrids with SiO_2 [Fig. 9B (b-d)], there exists both intramolecular [OH……N and NH……O] and intermolecular [OH……O and NH……O] hydrogen bonding between 2800-3000 cm^{-1} and 3300–3500 cm^{-1}, respectively. The compatibility of PBZ-SiO_2 is enhanced by these hydrogen bonding interactions[12,13].

The hydrogen bonding interactions in PBZ/SiO_2 hybrids was also confirmed by using XPS analysis.(Fig.10) PBZ/S5 hybrid shows peaks at 104.16 eV, which is slightly higher when compared with standard SiO_2 (103.77 eV). This shift in binding energy is due to hydrogen bonding interactions, as supported by FT-IR spectroscopy. Similar XPS shifts to higher binding energy were detected by Bigelow et al.[24,25]

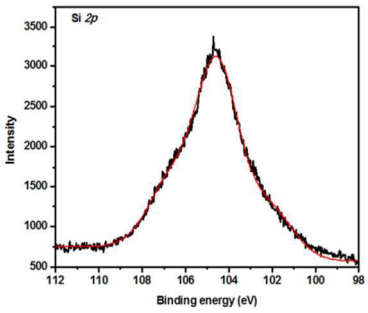

Figure 10: XPS of PBZ-SiO_2 (PBZ:S5)

Morphological studies

Figures 11 and 12 show the top – view scanning electron microscopy (SEM) and atomic force microscopy (AFM) images of the neat PBZ and PBZ/SiO_2 hybrids. As seen from Figure 10(a), the surface of the neat polybenzoxazine is much smoother than that of the nanocomposites. When compared with the flat polymer surface, the roughness of the PBZ-SiO_2 surface [Fig. 10 (b-d)] increased obviously with the addition of SiO_2 nanoparticles. This rough surface possessed both micro and nanoscale binary structure in which each micro island of the polybenzoxazine surface is covered with branchlike nanostructures. Such hierarchial morphology increases the surface roughness, thereby inducing hydrophobicity[23,26].

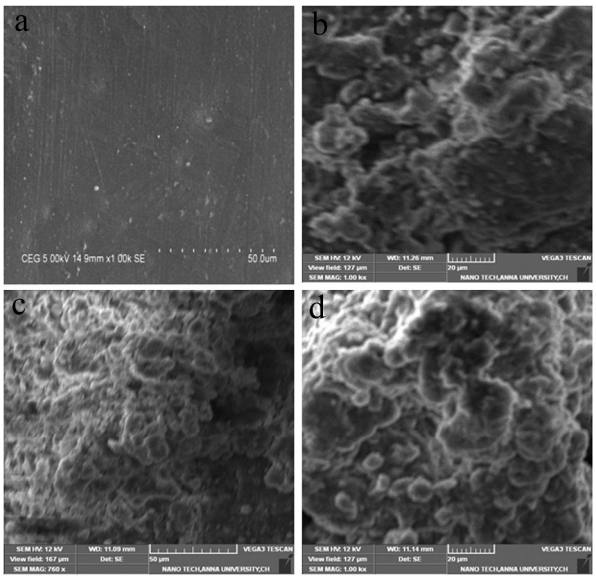

Figure 11: SEM images of PBZ-SiO_2 hybrids a) PBZ:S0; b) PBZ:S1; c) PBZ:S3 and d) PBZ:S5

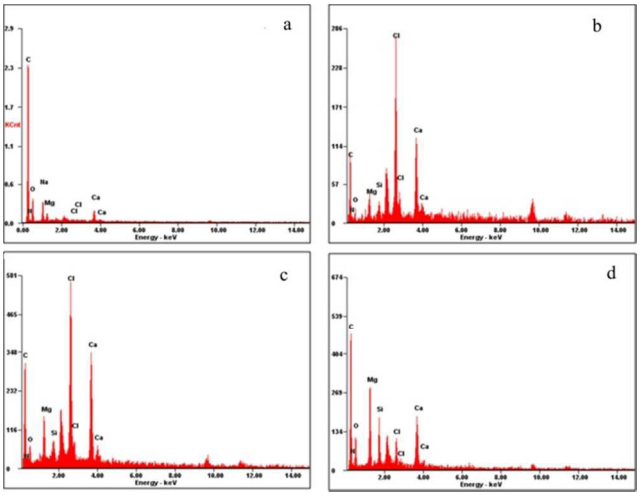

Figure 12: EDX images of PBZ-SiO_2 hybrids a) PBZ:S0; b) PBZ:S1; c) PBZ:S3 and d) PBZ:S5

The elemental composition of polybenzoxazines silica hybrids was analyzed using Energy dispersive X-ray spectroscopy (EDX), integrated with scanning electron microscopy. The presence of carbon, nitrogen, oxygen and silicon offers a good measure of the presence of silica and polybenzoxazine in the matrix as shown in fig.12.

The AFM images (Fig. 13) of polybenzoxazine and its nanohybrids indicate that the size of the nodules formed by the PBZ-SiO_2 particles are of uniform dimension showing uniform distribution as evidenced from SEM images.

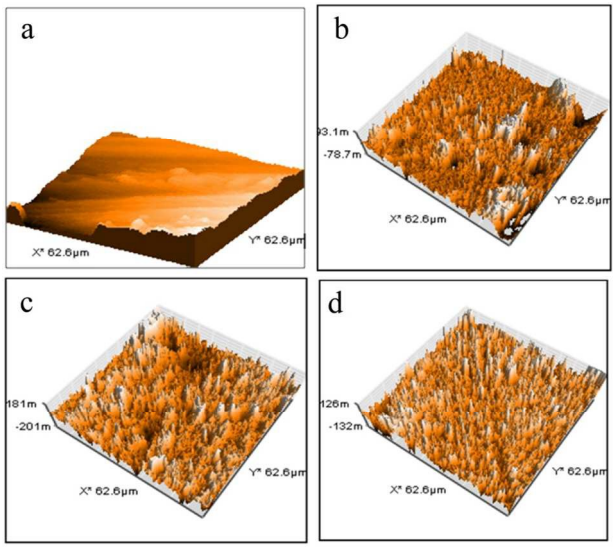

Figure 13: AFM images of PBZ-SiO_2 hybrids a) PBZ:S0; b) PBZ:S1; c) PBZ:S3 and d) PBZ:S5

The surface roughness of the polybenzoxazine silica hybrids was calculated from AFM measurements by using the equation given below,

$$R_t = R_p + R_v$$

Where, R_t is the total roughness of the sample measured R_p is the maximum profile peak height and R_v is the maximum profile valley depth.

The total roughness was found to be 7, 81, 108 and 134 nm for PBZ:S0, PBZ:S1, PBZ:S3 and PBZ:S5 respectively. The roughness value increases on increasing the silica content from 1 wt% - 5 wt%, which is in agreement with the AFM images.

HR-TEM was performed to analyze the microstructure of POSS–Pbz nanocomposites (Fig. 14). Dark spherical particles are found uniformly dispersed in the PBZ:S5 network, which are due to the presence of silica. These spherical particles are dispersed in nanometer range (about 20-30 nm in size) and there is no aggregation of the silica particles, showing uniform distribution.

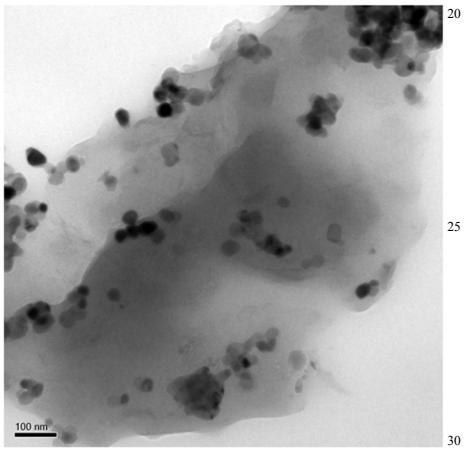

Figure 14: TEM images of PBZ-SiO_2 hybrids of PBZ:S5

Wetting behavior of PBZ/SiO_2 hybrids

Surface hydrophobicity of PBZ and its hybrids with nano SiO_2 was estimated by measuring the contact angles of water droplets on these surfaces as shown in Figure 15. In general terms, the contact angle of water is affected by surface properties, energy of materials and surface morphology. Larger contact angles imply more hydrophobic surfaces.[28]

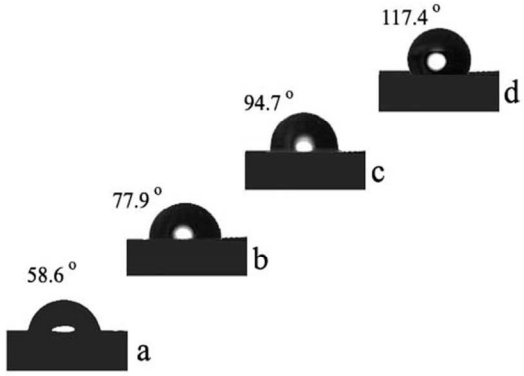

Figure 15: Optical images of water droplets on PBZ-SiO_2 hybrids a) PBZ:S0; b) PBZ:S1; c) PBZ:S3 and d) PBZ:S5

It is believed that rough surface has a higher hydrophobicity than the flat surface[2]. As shown in the figure, the polybenzoxazine – silica hybrids [PBZ:S1, PBZ:S3 and PBZ:S5] exhibit a linear increase in WCA from 58.6 – 117.4 °C[5,6].

The hydrophobicity of polybenzoxazine was improved by incorporation of SiO_2 nanoparticles even at low concentrations (say 5 wt% of SiO_2). The increased hydrophobicity of the hybrid [PBZ:S5] is ascribed to the trapped air in the interstices of the rough surface that prevents intrusion of water into the nanoparticles, resulting in an increase of water contact angle[11-13].

Dynamic Mechanical Analysis

Figures 16 and 17 illustrate the dynamic mechanical properties of the polybenzoxazine and nano silica filled polybenzoxazine hybrids. As seen from Fig. 13, at room temperature the storage modulus G' of the nano hybrids increased with increasing nano SiO_2 content. This is possible due to the more rigid characteristic of nanofiller. Additionally the storage modulus of neat polybenzoxazine (2.62 GPa) was enhanced in the presence of silica from 2.68 GPa (1 wt% of nano SiO_2) to 2.93 GPa (5 wt% of nano SiO_2)[5]. It could be noticed that even with only a small amount of nano SiO_2 in the hybrids, the mechanical properties were increased to a greater extent. Moreover, the strorage moduli values at high temperature, repersentative for the rubbery state increased remarkably as a result of the addition of nano SiO_2.

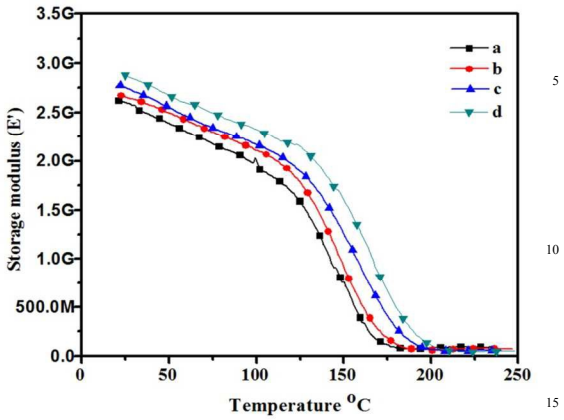

Figure 16: Storage modulus (from DMA) of PBZ-SiO_2 hybrids a) PBZ:S0; b) PBZ:S1; c) PBZ:S3 and d) PBZ:S5

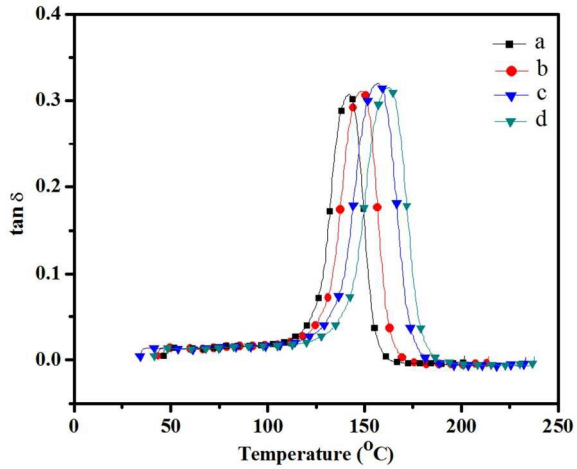

Figure 17: Loss modulus (from DMA) showing T_g of PBZ-SiO_2 hybrids a) PBZ:S0; b) PBZ:S1;c) PBZ:S3 and d) PBZ:S5

Influence is possibly attributed to the load transfer in the nanocomposite which occurs mainly through the filler nanoparticles[29]. The result also indicates that the reinforcing effect of the nanofiller was in both glassy and rubbery states, which implied strong interfacial bonding between the polymer and the reinforcing nano filler. Figure 14 shows the loss moduli G" curves of silica filled polybenzoxazine as a function of temperature[30-31]. The maximum peak temperature in the loss moduli curve is always taken as glass transition temperature (T_g) of the specimen as seen from the Figure 15. The T_g of neat polybenzoxazine (149 °C) was increased with increasing the amount of nano filler. The T_g of the nanohybrids at 5 wt% silica was found to be up to 164 °C. The increase of T_g is possibly due to the presence of the silica that offer resistance to the mobility of the polymer chains.

Crosslink Density

The crosslink density (CLD) or concentration of network chain γ_c is the number of moles of network chains per unit volume of the cured polymer. Crosslink density of highly crosslinked thermoset can be determined by modulus measurements in the rubbery plateau by using the equation of state for rubber elasticity[32] as,

$\gamma_c = \varepsilon'/3RT$

where,

ε' = tensile storage modulus in the rubbery plateau (from DMA)

T = temperature in K corresponding to the storage modulus value

R = gas constant

Table 2 shows the crosslink density of the PBZ/SiO_2 nano hybrids. It can be seen that the crosslink density obviously increases with increasing SiO_2 content in the nanocomposites. The enhancement in crosslink density is due to PBZ/SiO_2 acting as nanosized crosslinker in the matrix[33].

Thermogravimetric analysis

The thermal stability of PBZ/SiO_2 nanohybrids was investigated by TGA under nitrogen atmosphere. Figure 18 shows the thermograms and Table 2 lists the data obtained from these thermograms. By incorporating small amount of SiO_2 into the nanohybrids (5 wt %), the value of initial decomposition temperature (T_i) increased by 65 °C indicating that the nano – scale inorganic SiO_2 effectively improved the thermal stability of nanohybrids. The char yield values as characterized by percentage residues at 800 °C were also determined from TGA thermograms.

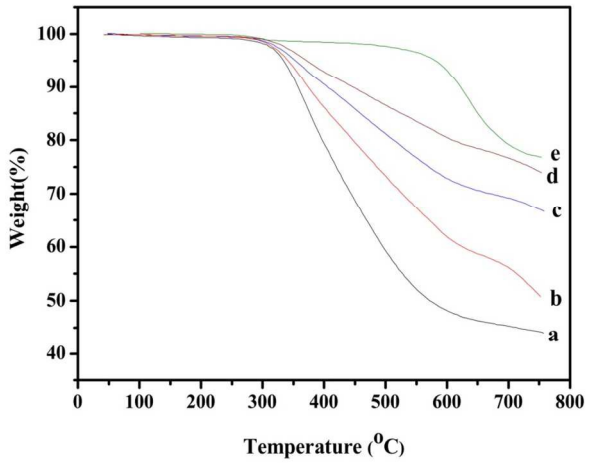

Figure 18: Thermal stabilities (from TGA) of PBZ-SiO_2 hybrids a) PBZ:S0; b) PBZ:S1; c) PBZ:S3 and d) PBZ:S5

A remarkable improvement of the char yield from 43% (neat PBZ) to 76% (5 wt% of SiO_2 incorporation) was observed for PBZ-SiO_2 nanohybrids. A possible reason is the high reactivity of SiO_2 molecules with good miscibility and uniform dispersion in the polymer matrix. The SiO_2 molecules act as cross-linking sites for the PBZ chain[34]. Furthermore, SiO_2 possesses low

S.No	Samples	SiO_2 (wt%)	DMA ε' (GPa)	T_g	CLD γ_e*10^{-5} (mol m^{-3})	TGA $T_{i\%}$ (^oC)	$T_{5\%}$ (^oC)	$T_{10\%}$ (^oC)	CY (%)	LOI
1.	PBZ:S0	0	2.62	149	3.4	297	331	394	43	34.7
2.	PBZ:S1	1	2.68	151	3.5	314	349	407	56	39.9
3.	PBZ:S3	3	2.81	157	3.7	343	391	447	68	44.7
4.	PBZ:S5	5	2.93	164	3.9	362	402	482	76	47.9

thermal conductivity due to the inorganic ceramic nature and intrinsic nano structure which could hinder the heat transfer to the materials and effectively retard the thermal degradation of weak bonds embedded within the network[53]. As a result, the thermal stability of the hybrid materials is enhanced. Moreover the surface of SiO2 was highly coated with PBZ which prevent the degradation of PBZ at lower temperature. Hence, the composites with higher SiO_2 content displayed significantly increased char yield, which is a direct indication of resistance to combustion. The improved thermal stability is a result of the combined effects of higher aromatic and silica contents which increased the crosslink density thereby increasing thermal stability[36].

Flame retardancy

The non-flammability of neat PBZ and PBZ-SiO_2 hybrids is explained in terms of the value of limiting oxygen index (LOI). LOI is defined as the minimum fraction of oxygen in a mixture of O_2 and N_2 that will support flaming combustion. The LOI values were calculated from the char yields obtained from TGA analysis by using Van Krevelan and Hofytzer equation[37] as shown below,

LOI = 17.5 + 0.4 (CY)

Where,

LOI is the limiting oxygen index

CY is the char yield (from TGA data)

The LOI value for PBZ-SiO_2 nanohybrids reinforced with 0, 1, 3 and 5 wt% of SiO_2 are 34.7, 39.9, 44.7 and 47.9, respectively as shown in Table 2. The LOI value obtained for the nanohybrids are all above the threshold value of 26. This shows that the incorporation of SiO_2 into PBZ-SiO_2 hybrid system results in thermoset with good self extinguishing and flame retardant properties[38,39].

Remarks and Conclusions

Thermal curing method was adopted for the fabrication of polybenzoxazine/silica nanohybrids. SEM and AFM analysis reveals the formation of hierarchical structures possessing both micro- and nano- sized roughness. It is found that by tuning the surface composition, the hydrophobicity of the hybrids increased from 58.6^o [for neat PBZ] to 117.4^o [for PBZ:S5]. In addition to increased hydrophobicity, the polybenzoxazine silica hybrid [PBZ:S5] also exhibits high thermal [$T_{5\%}$ = 402 ^oC] and mechanical [storage modulus = 2.93 GPa] stability. These enhancements in thermo-mechanical properties are the results of subsequent cross-linking with control in the extent of inter and intramoleculary hydrogen bonding interactions. In summary, a simple and inexpensive method has been described in this paper, and the results obtained are significant in terms of their importance to academic and industrial applications.

Notes and references

1. C. F. Wang, T. Wang, C. S. Liao, S. W. Kuo and H. C. Lin, *J. Phys.Chem. C*, 2011, **115**, 16495.
2. L. Shena, H. Dinga, W. Wanga and Q. Guob, *Appl. Surf. Sci.*, 2013**, 268**, 297.
3. C. F. Wang, Y. T. Wang, P. H. Tung, S. W. Kuo, C. H. Lin, Y. C. Sheen and F. C. Chang, *Langmuir*, 2006**, 22**, 8289.
4. H. Ogihara, J. Xie and T. Saji, *Colloids and Surfaces A: Physicochem. Eng. Aspects*, 2013, **434**, 35.
5. C. S. Liao, C. F. Wang, H. C. Lin, H. Y. Chou and F. C. Chang, *Langmuir*, 2009, **25**, 3359.
6. Raza, Y. Si, B. Ding, J. Yu and G. Sun, *J. Colloid Interface Sci.*, 2013, **395**, 256.
7. W. Hou and Q. Wang, *Langmuir*, 2007**, 23**, 9695.
8. S. W. Kuo, Y. C. Wu, C. F. Wang and K. U. Jeong, *J. Phys. Chem. C*, 2009, **113,** 20666.
9. C. Jubsilp, T. Takeichi, S. Hiziroglu and S. Rimdusit, *Polym. Eng. Sci.*, 2009, **49**, 1022.
10. C. F. Wang, S. F. Chiou, F. H. Ko, C. T. Chou, H. C. Lin, C. F. Huang and F. C. Chang, *Macromol. Rapid Commun*., 2006, **27**, 333.
11. T. H. Kao, J. K. Chen, C. C. Cheng, C. I. Su and F. C. Chang, *Polym. J.*, 2013, **54**, 258.
12. J. Liu, X. Lu, Z. Xin and C. Zhou, *Langmuir*, 2013, **29**, 411.
13. C. Zhoua, X. Lua, Z. Xina, J. Liua and Y. Zhang, *Prog. Org. Coat.*, 2013, **76**, 1178.
14. B. Kiskan, F. Dogan, Y. Y. Durmaz and Y. Yagci, *Designed Monomers and Polymers*, 2008**, 11**, 473.
15. P. Thirukumaran, A. Shakila Parveen and M. Sarojadevi, RSC. Adv., 2014**, 4**, 7959.
16. C. P. Yang, R. S. Chen and K. H. Chen, *J. Appl. Polym. Sci.*, 2005, **95**, 922.
17. D. Yina, Y. Lia, H. Yang, S. Yang, L. Fan and J. Liu, *Polym. J.*, 2005, **46**, 3119.

18. T. Agag, L. Jiu and H. Ishida, *Polym. J.*, 2009, **50**, 5940.
19. Y. Liu, C. Yue and J. Gao, *Polym. J.*, 2010, **51**, 3722.
20. T. Agag and T. Takeichi, *Macromolecules*, 2003, **36**, 6010.
21. S. Li, S. Yan, J. Yu and B. Yu, *J. Appl. Polym. Sci*., 2011, **122**, 2843.
22. Z. Xiaoqing, M. G. Looney, D. H. Solomon and A. K. Whittaker, *Polym. J.*, 1997, **38**, 5835.
23. M. C. Tseng and Y.L. Liu, *Polym. J.*, 2010, **51**, 5567.
24. R. W. Bigelow, K. Y. Law, P. H. K. Pan, and H. J. Freund, J. Electron Spectrosc. Relat. Phenom. 1988, 46,1.
25. S. J. Kerber, J. J. Bruckner, K. Wozniak, S. Seal, S. Hardcastle, and T. L. Barr J. Vac. Sci. Technol. A 199614(3), 1314.
26. C. Liu, D. Shen, R. M. Sebastian, J. Marquet and R. Schonfeld, *Macromolecules*, 2011, **44**, 4616.
27. M. Raposo, Q. Ferreira and P. A. Ribeiro, *Modern Research and Educational Topics in Microscopy*, 2007, 758.
28. M. Wang, C. Chen, J. Ma and J. Xu, *J. Mater. Chem.,* 2011, **21**, 6962.
29. J. Zhang, R. Xu and D. Yu, Eur. *Polym. J*., 2007, **43**, 743.
30. Q. Chen, R. Xu, J. Zhang and D. Yu, *Macromol. Rapid Commun*., 2005, **26**, 1878.
31. K.W. Huang and S.W. Kuo, *Macromol. Chem. Phys*., 2010, **211**, 2301.
32. D. Wenjie, S. Jiajia, W. Yixian, X. Riwei and Y. Dingsheng, *Mater. Des*., 2010, **31**, 1720.
33. V. H. Pedro, D. Kazuo, A. Hiroshi and H. Ishida, *Macromolecules*, 2008, **41**, 9704.
34. G. Yang, Z. Xue, Q. Zhunag, X. Liu, K. Zhang and Z. Han, *Synth.Met.*, 2013, **175**, 112.
35. R. Tamaki, Y. Tanaka, M. Z. Asuncion, J. Choi and R. M. Laine, *J.Am. Chem. Soc.*, 2001, **123**, 12416.
36. L. Marta, P. S. Mercedes, A. G. Francisco and S. Roberto, *J. Mater. Chem.*, 2011, **21**, 12803.
37. Y. Yusuf, K. Baris, G. Narendra Nath, *J. Polym. Sci., Part A: Polym. Chem.*, 2009, **47**, 5565.
38. C. L. Chiang and M. C. Ma, *Polym. Degrad. Stab.*, 2004, **83**, 207.
39. D. W. Van Krevelen, *Polym. J.*, 1975, **16**, 615.